

Molecular Electronics: Effect of external electric field

S. Lakshmi, Sudipta Dutta and Swapan K. Pati

Theoretical Sciences Unit

Jawaharlal Nehru Center for Advanced Scientific Research

Jakkur Campus, Bangalore 560 064, India.

Abstract

The effect of electric field, applied on systems in the nanoscale regime has attracted a lot of research in recent times. We highlight some of the recent results in the field of single molecule electronics and then move on to focus on some of our own results in this area. We have first shown how important it is to obtain the spatial profile of the external bias potential across the system, and how this would change in the presence of electron-electron interactions. We have also studied different kinds of insulators in the presence of the spatially varying external bias, and have explicitly shown that a two sublattice structure, caused either by a lattice distortion, or by the presence of substituents with strong dipolar nature, can result in negative differential resistance (NDR) in the transport characteristics. We also find this to be true in case of correlated insulators. Additionally, we have shown clear NDR behavior in a correlated double quantum dot by tuning the electron-electron interaction strength in the system.

I Overview

Research in the field of nanoscience has seen an upsurge in recent times, largely owing to the fact that silicon electronics is fast approaching a road-block, dictated by both the laws of physics as well as the cost of production. All these years, the semiconductor microelectronics industry has always been driven by the need for powerful computational devices with high computing speeds. Until now, this has been achieved through the ‘top down’ lithographic approach which involves the miniaturization of existing silicon-based chips. Gordon Moore, in 1965, in his famous ‘Moore’s law’, predicted that there would be a doubling of devices per chip every 18 - 24 months [1], and this has held true over the past three decades. However, the ‘top down’ approach is expected to reach its physical limit in the next few years owing to certain factors. This rate of downscaling is expected to hamper the performance of these devices, as issues related to quantum tunneling, interconnect delays, gate oxide reliability, and excessive power dissipation would start playing a major role at such small length scales. The electronic properties of semiconductor structures fabricated via conventional lithographic processes are also quite difficult to control at the nanometer scale. Although some of these issues can be overcome by improving the device design, the increasing cost of fabrication has motivated research in other directions [2]. It has led to the replacement of the ‘top-down’ lithographic approach by a ‘bottom-up’ synthetic chemical approach of assembling nanodevices and circuits, directly from their molecular constituents, leading to the next generation of electronics, now known as ‘molecular electronics’.

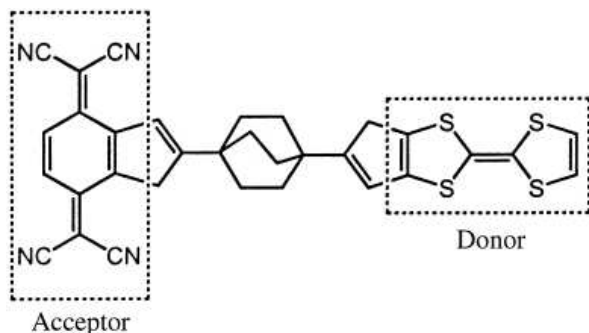


Figure 1: Organic analogue of a p - n junction, composed of a donor moiety tetrathiafulvalene (TTF) connected by a methylene bridge to an acceptor moiety tetracyanoquinodimethane (TCNQ) (taken from ref. [5]).

Almost all electronic processes in nature occur in molecular structures, which are typically of the order of a few nanometer, and hence already possess a natural scale for use as functional nanodevices. Their abilities of selective recognition and self-assembly helps make molecular building blocks through cheap methods of fabrication. Molecules can also exhibit several stable geometric structures or isomers, having very different optical and electronic properties. Their conformational flexibility can also give rise to interesting transport properties, and a simple manipulation of their composition and geometry can lead to a wide variety of binding, optical and structural properties, which can be efficiently tuned to our needs [3, 4]. Moreover, in comparison with molecules, solids have the distinct disadvantage that it is relatively difficult and expensive to fabricate them into many millions of nearly identical structures, as required in each dense computer chip. All these features make molecules ideal candidates for electronics applications, and there is a growing recognition of this in the past decade.

The first suggestion, that molecules could indeed be used as alternatives

to silicon chips came from Aviram and Ratner [6] who, in 1974, discussed theoretically the possibility to construct a molecular rectifier, based on a single organic molecule. They suggested that a single molecule with a donor(D)-spacer-acceptor(A) structure (Figure 1) would behave as a p-n junction diode when placed between two electrodes. This hypothesis remained so, until more than 20 years later, Metzger [7] studied Langmuir-Blodgett (LB) films of γ -(n-hexadecyl) quinolinium tricyanoquinodimethanide (D- π spacer-A species) between metal electrodes and demonstrated rectifying behavior. Over the years, with the advent of the scanning probe microscopy and other techniques, researchers have developed ways of addressing, imaging, manipulating, and performing measurements on molecules connected between metal leads. Advances in synthesis of organic molecules, their assembly and measurement has also led to an increasing interest in the field of molecular electronics. Charge transport through molecules can now be probed in a controlled way and several prototype devices such as conducting wires, rectifiers, switches, and transistors have already been demonstrated, as detailed below.

In 1997, Reed et al. measured the conductance of a single molecule of benzene-1,4-dithiol in a mechanically controllable break junction [8], where a single organic molecule was adsorbed in an adjustable tunnel gap formed by mechanically breaking a metal wire on a substrate. More complex anthracene based molecules were later studied by Reichert et al. using the same method and wire and diode like properties were demonstrated in symmetric and asymmetric molecules respectively [9]. Kushmerick and co-workers used the crossed wire method to measure transport through symmetric and asymmetric oligo-phenylene-ethynylenes (OPEs), observing molecular wire and

diode features in their respective I-V characteristics [10]. Reed and Tour et al. discovered very interesting negative differential resistance (NDR) behavior in these OPEs, functionalized by NH_2 and NO_2 groups, triggering a gamut of experimental and theoretical studies to understand the phenomenon, as will be elaborated later. A related molecular response to an external electric field is that of switching, which is a very useful property in the design of logic based molecular devices. In this regard, the most popular class of molecules are catenanes and rotaxanes which have shown possibilities for being used as switching devices. Molecules such as bipyridyl-dinitro oligophenylene-ethynylene dithiol (BPDN-DT) [11] and thiol substituted oligoaniline [12] molecules have also been demonstrated to show bistable conductance switching behavior. pH [13] and photo induced [14] molecular switching have also been observed in some molecules. The other most challenging and yet most critical step towards the ultimate goal of molecular electronics, is the demonstration of a molecular field-effect transistor (FET). Even this has been made possible by Xu et al., who have described such a device made of perylene tetracarboxylic diimide, where they showed how a variation in the electrochemical gate voltage could result in a 1000 fold increase in the source-drain current, just like in a n-type FET [15].

Single electron transistor (SET) behavior has already been observed in transport through semiconductor quantum dots, metallic and semiconducting nanoparticles, and even in single π -conjugated organic molecules with several distinct charged states which can control its transport properties. Carbon nanotubes, fullerenes and semiconductor nanowires represent another set of interesting systems which have been shown to exhibit Coulomb Blockade

[16, 17], Kondo behavior [18, 19] and have also been fabricated into FETs [20] and non-volatile memory elements. Apart from these, bio molecules, which have both natural self-assembly and self-recognition properties, have become popular candidates for electronics applications. A large number of transport measurements have been performed on DNA, the blueprint of life, which have reported results ranging from conducting, semi-conducting to even insulating behavior [21, 22, 23, 24, 25], depending on experimental methods, surrounding structures, solvents used etc. A protein based field-effect transistor (Pro-FET) based on the blue copper protein azurin has also been demonstrated to operate at room temperature and ambient pressure [26].

A. Theoretical issues

Although there has been such a quantum increase in the experimental demonstration of prototype molecular devices, a theoretical understanding is challenged by a number of fundamental issues. A nanoscale molecule between macroscopic electrodes is in a complete state of non-equilibrium, with each of the source and drain contacts trying to bring the molecule into equilibrium with its electrochemical potential, thus driving current through the system. The problem presents many characteristic length scales, defined to truly determine when the classical regime ends and the quantum regime begins. These are the Fermi wavelength, the momentum relaxation and phase relaxation lengths, which gain prominence in this length scale [27, 28]. Since the system is confined in one or two directions, the quantum modes in the directions normal to the electron propagation direction are discretized, depending on the Fermi wavelength. It was shown by Landauer [29] that the

conductance of a nanoscale system depends on the transmission probabilities of electrons through these modes, resulting in quantization of their conductance. A changing width hence results in steps in the conductance as opposed to continuous dependence of conductance on dimensions in macroscopic conductors. The momentum and phase relaxation lengths determine how far the electrons in the system would travel, before collisions would make them lose memory of their initial momentum and phase, respectively. While the former can change the current-voltage response of the device quite drastically due to impurity scatterings, the latter could take the conduction from a incoherent classical transport to a coherent transport where quantum interference effects would play a very significant role. Classical transport, which occurs when the length of the conductor is greater than both the momentum and phase relaxation lengths, resembles transport that we are very familiar with in the macroscopic regime, obeying the well-known Ohm's law. At the other extreme, when the system under consideration is smaller than both these length scales, transport is known to be ballistic, where the rate of transport is independent of the length of the system and described by the Landauer's formula in terms of transmission probabilities as:

$$G_c = \frac{2e^2}{h}MT \quad (1)$$

Here, the conductance scales linearly with the transmission (T) and the number of eigenmodes (M) in the wire. Interestingly, the conductance of even a ballistic sample is finite, due to the resistance at the interface between the small system and the large contacts [27]. Measurements on atomic point con-

tacts and metallic carbon nanotubes have already demonstrated this behavior where the transmission of each available channel is nearly unity. However, in general, the molecular eigenstates are not fully delocalized leading to a transmission that might be less than unity. The other regime, where momentum changes occur from impurity scatterings, but with phase maintenance, results in a coherent but diffusive transport. The rate of electron transfer in this case is exponentially dependent on the length of the molecular bridge. This mechanism holds, especially for short wires with large HOMO-LUMO gaps such as oligoalkanes. It is also known sometimes as “superexchange” where the electron transfer proceeds through “virtual” orbitals, which are energetically well-separated from the Fermi levels of the electrodes. In addition to all these, conduction could also be mediated by quasiparticles like solitons and polarons in the molecule.

Apart from length scales that differ markedly when one goes from a macroscopic to a nanoscale conductor, the energy scales of the whole system consisting of the molecule with its discrete energy levels attached to macroscopic metallic electrodes with a continuous band structure, poses much of the challenge in understanding molecular electronic transport. Some of the issues that one encounters in this regard are [30] (a) *Electrode-molecule coupling and contact surface physics* which determine the broadening of the molecular energy levels and hence the lifetime of the electron in those levels as well as where the Fermi energy of the electrode would align with respect to the molecular levels (b) *Electronic structure of the molecule* which decides the nature of the molecular orbitals and hence their transmission probabilities (c) *Device electrostatics* or how the applied external electric field would

impact the device energetics (d) *Inelastic and thermal effects* which come into play when strong electron-electron and electron-phonon interactions are present in the molecule. The most widely employed method for calculating non-equilibrium transport in such nanoscale systems, with consideration of most of these issues mentioned above, is the Non-equilibrium Green's function formalism (NEGF) [28], which for the case of coherent transport boils down to the Landauer's formalism for calculating current [31]:

$$I = \frac{2e}{h} \int_{-\infty}^{\infty} dE \operatorname{Tr}[\Gamma_L G \Gamma_R G^\dagger] (f(E, \mu_L) - f(E, \mu_R)) \quad (2)$$

Here G represents the device Green's function, $\Gamma_{L,R}$, the imaginary part of the self-energies correspond to the broadening of the molecular energies, and $f(E)$ represents the Fermi-Dirac distributions at the two electrodes with electrochemical potentials μ_L and μ_R . The NEGF formalism has been combined with many semi-empirical and Hartree Fock methods to obtain the current-voltage characteristics of molecules. Transport calculations have also been incorporated into electronic structure methods and packages such as TRAN-SIESTA [32], Atomistix toolkit (ATK), WanT [33], McDCal [34], Gaussian embedded cluster method [35] etc, which have become very popular in present times.

In this article, we discuss various aspects of a molecule connected between macroscopic electrodes. In section II, we briefly discuss the effect of external electric field on the potential profile in an interacting molecular wire. In section III, we introduce the phenomenon of negative differential resistance in single molecular junctions, and detail the experimental and theoretical

efforts over the last few years in understanding the phenomenon. We will then elaborate our work on this interesting device behavior, focusing on the effect of dimerization and donor-acceptor groups in causing NDR. The insight that we have gained from our work on NDR in molecular systems (which are primarily insulating due to their finite sizes), resulted in studies on the effect of electric field on insulators formed out of the strong electron-electron interactions in them (such as the Mott insulators). This part will be briefly described in section IV. In section V we give a detail description of NDR in the coulomb blockade regime in molecular quantum dots. Finally, we conclude with the summary of results and discuss the future outlook.

II The potential profile in an interacting molecular wire

As was discussed before, a variety of factors have been found to be very crucial in determining the nature of current-voltage characteristics in nanoscale systems, like the electronic structure of the constituent molecule, the interface physics and the profile of the potential drop across the molecule between the electrodes. This latter point, in itself, is very interesting to probe, as most often, it is not the low bias or linear response characteristics of a wire that are interesting, but rather the full current-voltage characteristics. The low-bias response would be determined simply by the equilibrium electronic structure and energies, but the device characteristics at larger voltages would require one to understand in detail the nature of the potential profile inside the molecule in response to an externally applied voltage.

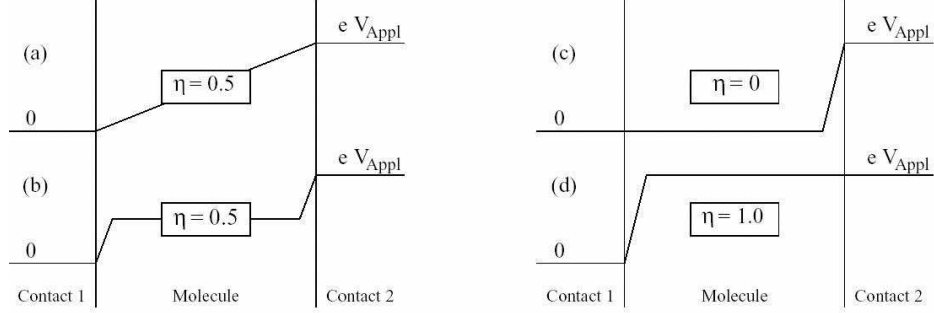


Figure 2: Examples of a few potential profiles in terms of the parameter η (taken from reference [30]).

Datta et al. [30, 36] suggested a one parameter characterization of this potential profile, through the voltage division factor η ($0 < \eta < 1$), which rigidly changes the molecular energies by ηeV or equivalently, shifts the electrochemical potential of the left and right electrodes as $\mu_L = E_F - \eta eV$ and $\mu_R = E_F + (1 - \eta)eV$. Figure 2 shows few examples of the potential profile obtained by varying the values of η . They found that this parameter has a profound effect on the molecular current-voltage characteristics. A value of $\eta = 0.5$ occurs when the molecule is coupled equally to both electrodes, however as shown in Figure 2 (a) and (b), it could still result in two different potential profiles depending on the extent of charging in the molecule. The current through the molecule, in this case, especially at low bias, would be nearly symmetric. Values of $\eta = 0$ and 1 appear when the coupling to the contacts are unequal. This would result in a I-V curve whose positive branch would look very different from the negative one.

Most of the earlier calculations in this field assumed the electrostatic potential profile due to the applied bias to be a ramp (linear) function. This is equivalent to assuming that all the charge is localized only in the external

boundaries, neglecting any effects due to screening. However, at high bias, there could be a temporary accumulation of charge on the bridge, which would screen the external field and hence result in a profile with non-uniform field gradient. To account for this, Mujica et al. have proposed a self-consistent solution of Poisson equation coupled with the Schrödinger equation [37] and suggested that this is essential to account for the actual features of the current spectra of these nanowires. In our studies [38], we have included this aspect while recognizing the effects of electron-electron interactions on the potential profile across a molecular wire, assumed to be a one-dimensional chain of N atoms with one orbital per atomic site. We assume a Hubbard model to describe the system as

$$H = \sum_i \sum_{\sigma} -t(a_{i\sigma}^{\dagger}a_{i+1\sigma} + hc) + U \sum_i n_{i\uparrow}n_{i\downarrow} \quad (3)$$

where t is the electron hopping term and U is the Hubbard on-site electron repulsion term. To solve this Hamiltonian in the mean-field limit with electronic spins explicitly, we consider the averaged mean-field quantities, $\langle a_{i\sigma}^{\dagger}a_{i\sigma} \rangle$ and $\langle a_{i\sigma}^{\dagger}a_{i-\sigma} \rangle$ [39, 40]. The averaged (mean-field) form of the Hamiltonian can then be written in terms of these mean-field quantities as,

$$H_{mf} = -t \sum_i (a_{i\sigma}^{\dagger}a_{i+1\sigma} + hc) + U \sum_{i\sigma} a_{i-\sigma}^{\dagger}a_{i-\sigma} \langle a_{i\sigma}^{\dagger}a_{i\sigma} \rangle - U \sum_i (\langle a_{i\sigma}^{\dagger}a_{i-\sigma} \rangle a_{i\uparrow}^{\dagger}a_{i\downarrow} + hc). \quad (4)$$

Note that, the second U term in eqn. (4) destroys the spin conservation and would only contribute if the system has a nonzero finite magnetization. In

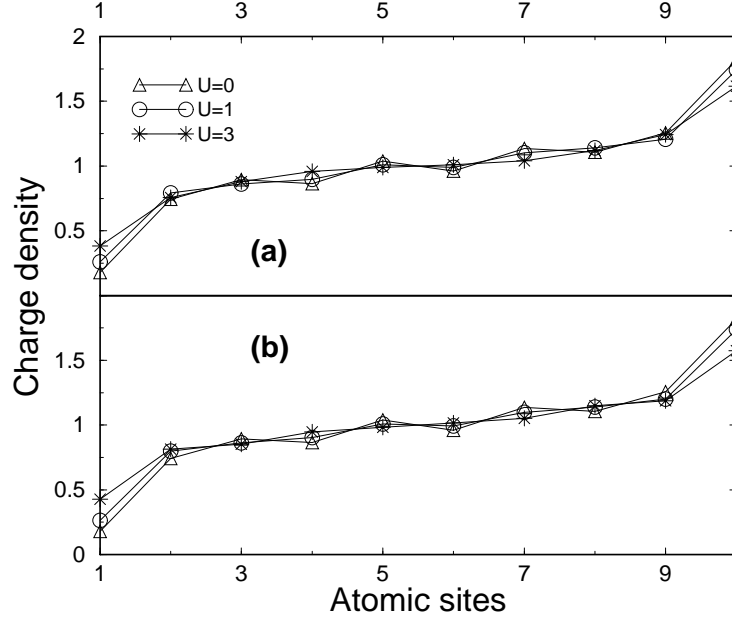


Figure 3: Comparisons of charge densities as a function of atomic sites for various U parameters with mean-field (a), and exact (b) methods, calculated at a bias of 6V.

our case, however, we consider the chain of N atoms with $N/2$ up spins and $N/2$ down spins, so that the ground state magnetization is zero. Therefore, although this term does not contribute for our system, the term is explicitly given since the Hamiltonian describes the general mean-field derivation of the Hubbard model.

The electric field applied on the wire adds the term $\sum_{i,\sigma} F_i a_{i\sigma}^\dagger a_{i\sigma}$ to the Hamiltonian, where the variation of the field F with the site index i is the potential profile we are interested in. We start our calculations by assuming that the electrostatic field is a linear ramp function across the metal-molecule interface. By solving the mean-field Hamiltonian, we obtain the charge density (ρ_i) at every site, given by $\rho_i = \sum_{\sigma} a_{i\sigma}^\dagger a_{i\sigma}$. This becomes the input for

the one-dimensional Poisson equation,

$$F_{i+1} + F_{i-1} - 2F_i = -\rho_i \quad (5)$$

where the inter-atomic distance and the dielectric constants at every atomic site are assumed to be constant and unity. Additionally, unlike previous self-consistent studies [37], where the boundary conditions for solving the Poisson equation was considered by assuming finite but large dielectric constants for the metal electrodes as compared to the molecular sites, here we enforce that the left electrode (to which the atomic site “1” is weakly coupled) has zero bias while the right electrode has the full bias (ie, F). This ensures that the electrodes are not polarized due to charge accumulations at the molecular sites. We then solve the modified Hamiltonian $\tilde{H}_{ii} = H_{ii} - eF_i$, self-consistently with the Poisson equations using the appropriate boundary conditions, until the charge densities and the site potential fields converge.

Since our calculations are performed in the mean-field, we have also compared our results with those obtained by performing exact diagonalization calculations. Our charge density calculations on a 10 site half-filled system, with various values of the Hubbard strength U , shows uniform density in the middle of the chain (with alternations in the ends due to boundary effects), at zero bias. However, with increasing bias, as shown in Figure 3, a depletion of charge densities in one end, and an accumulation in the other, ensues. Furthermore, the induced polarization due to the external field decreases with increase in U . This is quite easy to understand, since, increase in U localizes the charges, and so the effective field that the system experiences is smaller

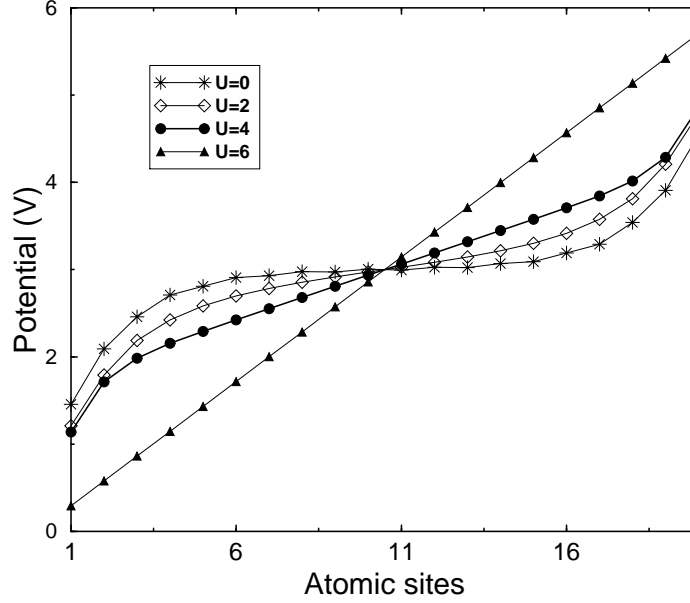


Figure 4: Spatial electrostatic potential profile across the electrode-molecule interface, for various U values, calculated at a bias of 6V.

for larger U values. It can also be seen that for all values of U , the mean-field charge densities compare fairly well with the exact calculations.

In Figure 4, we present the self-consistently derived potential profile for a chain of 20 sites, with different U . At the outset, our calculations show that for a tight-binding molecule ($U = 0$), the potential has the features which has been described by others [37], in which most of the voltage drop occurs near the electrodes, and is essentially constant (zero gradient) in the wire region (which we will call the tight binding potential profile or TBPF). The tight-binding solutions are plane-waves wherein electrons are completely delocalized all over the molecule. The inclusion of a finite Hubbard repulsion is known to induce Mott localization, and the potential differs from the tight-binding solution, with the gradients becoming nonzero in the middle of the molecule. The general feature, hence shows that, increasing the value of U

from small to large takes the potential profile slowly from TBPF to ramp spatial variation. This is because large U introduces strong site localization and the electrons are essentially “particle-like” in the large U limit. Hence the external field is not able to induce much accumulation of excess charge in the system, thus retaining the ramp nature of the potential profile.

These studies give an idea of how interactions in a nanoscale system can change the nature of the potential profile across it, which is expected to have a lot of implications in its current-voltage characteristics also.

III Negative Differential Resistance

Negative differential resistance (NDR) behavior, is a property of electrical circuits in which, over certain voltage ranges, current is a decreasing function of voltage. Semiconductor devices exploiting this effect are widely used to make amplifiers and oscillators, however, it was reported for the first time in molecular systems, by Reed and Tour et al. in oligo(phenylene-ethynylenes) (OPEs), functionalized by amine (NH_2) and nitro (NO_2) substituents [41]. This molecule shown in Figure 5, consists of three benzene rings connected by triple bonds, with donor (NH_2) and acceptor (NO_2) groups (or sometimes only the acceptor) in the middle ring. The strong NDR peak with a peak-to-valley ratio (PVR) of 1030:1 was observed at 60K, and was found to reduce with increasing temperature [42]. They also reported electronically programmable memory behavior in the NO_2 functionalized devices [43], using the nanopore setup for performing experiments. Very recent studies performed by Tao et al., using a STM break junction method where a Au

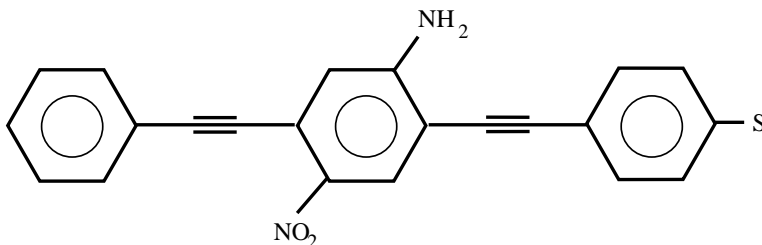


Figure 5: The Tour molecule consisting of three benzene rings connected by triple bonds with donor (NH_2) and acceptor (NO_2) substituents in the middle ring.

tip was driven into contact with a Au surface in a solution containing the organic molecules have proven to be very effective *single* molecule junctions. The conductance was then measured as the tip was retracted. Their experiments also confirmed earlier observations by indicating sharp NDR peaks in the NO_2 functionalized OPEs [44]. NDR response has also been reported in ferrocenylundecanethiol self-assembled monolayers [45], azobenzene molecular junctions [46], oligopeptides [47], C_{60} encapsulated double walled carbon nanotubes [48], bilayer junctions formed by nitro substituted OPE and an alkanethiol [49], and even in molecules on doped silicon surfaces [50].

A large number of theoretical studies has also been performed on many molecules to understand the underlying causes for molecular NDR behavior, sometimes leading to even predictions of NDR in some novel molecules. Theoretical predictions of NDR on systems include carbon atomic wires [51], metallic and semiconducting clusters [52], molecules between transition metal contacts [53] and some organometallic molecules [54]. Considerable amount of theoretical work based on semi-empirical and *ab-initio* methods have also been performed to understand NDR behavior in the Tour molecules. Many explanations for this phenomenon based on charging [55, 56, 57], reduction

of the acceptor moiety [58], twisting of the ring structure leading to conformational changes [59, 60, 61, 62], bias driven changes in molecule-electrode coupling [63] etc, have been proposed. However, most of these require to impose some external factors like the rotation of the middle ring, or introduction of extra charge in the molecule in order for the external bias to cause NDR at some bias. Also, most often they do not make a relation between structural preference and bias polarity and hence do not explain the asymmetry that has been observed in the experimental I-V characteristics. In our studies on this phenomenon, we have used simple, but insightful models to understand the NDR behavior. Our study involves two aspects of these molecules (a) conjugation or dimerization (b) presence of donor-acceptor substituents and their respective roles in taking the molecule through a negative differential resistance, when subjected to an external electric field.

A. Role of dimerization (lattice distortion)

It is well-known that a half-filled one-dimensional metal, due to the effects of strong electron-phonon coupling, is unstable against Peierls distortion, producing a finite charge gap in the system, thereby lowering the energy of the occupied states and stabilizing the distortion [64]. The competition between the lowering of the electronic energy and the increase of the elastic energy due to distortions often leads to modulation of the bond lengths in the system, removing high density of states at the Fermi surface.

For such low-dimensional systems, the approximation that the electron transfer occurs through purely the electronic states, completely ignoring the change in underlying lattice structure during the transfer, is not valid. There

have been many studies on the inelastic conductance through molecular wires in the presence of vibrational modes by Ness, Fisher [65], May, Todorov, Segal, Nitzan [67] and others before. However, in our study, the assumption of strong coupling between the molecule and electrodes suggests that the electron traversal time is large and hence we neglect possibilities of dephasing due to electron-phonon interaction. The time scale is also too short for the electron to remain on the molecular bridge and hence form a polaron. However, the net effect of the interaction is to distort the molecular bridge resulting in modified electron hopping strengths. In this study [68], hence, we have considered transport properties purely in the presence of underlying lattice distortions. We describe the finite wire within the Su-Schreiffer-Heager (SSH) model, where the electrons are treated using a tight-binding description and the lattice degrees of freedom are treated adiabatically[69, 70]. The interaction between the wire and electrode are considered through the Newns-Anderson chemisorption model [71, 72] and the nonlinear response of the current with the applied bias calculated using the Landauer's formalism. The Hamiltonian is given by:

$$H = \sum_i -(t + \alpha(u_i - u_{i+1}))(a_i^\dagger a_{i+1} + hc) + \frac{1}{2}K \sum_i (u_{i+1} - u_i)^2 \quad (6)$$

where the first term describes the hopping of π electrons along the polyene chain without spin flip, the second term corresponds to the π electron-phonon interaction, and the last term is the phonon Hamiltonian. t is the nearest neighbor hopping integral and K and α are the elastic spring constant associated with the nuclear motion and the electron-phonon coupling strength

respectively. In this Hamiltonian, the hopping strengths are linearized, i.e, the strength of the hopping is proportional to the difference in displacements u_i of the atoms from their mean positions. The Hamiltonian can be re-written as $H = \sum_i -(1 + \delta_i)(a_i^\dagger a_{i+1} + hc) + \frac{1}{\pi\lambda} \sum_i \delta_i^2$ where $\delta_i = \frac{\alpha(u_i - u_{i+1})}{t}$ and λ is a dimensionless coupling constant defined as $\lambda = \frac{2\alpha^2}{\pi K t^2}$, which we will use in our calculations as a measure of the electron-phonon coupling strength. We minimize the above Hamiltonian with the constraint that the energy changes associated with the net displacement about the mean positions should be zero so that the total length of the wire remains constant, i.e, $\sum_i \delta_i = 0$. Minimizing it with respect to the δ_i gives an expression for the δ s, the energy shift of the i^{th} bond from its equilibrium value,

$$\delta_i = \frac{\pi\lambda}{2} [\langle a_i^\dagger a_{i+1} + hc \rangle - \frac{1}{N} \sum_i \langle a_i^\dagger a_{i+1} + hc \rangle] \quad (7)$$

where N is the total number of bonds. We have calculated these δ s, first, for an isolated wire consisting of 20 sites for a range of electron-phonon coupling strengths. We find that as the coupling strength is increased, the chain is more and more distorted (dimerized), however, in this process, the system gains some additional energy, and opens up a gap about the Fermi energy thereby making the system insulating. This is the Peierls dimerization mechanism. This nonconducting gap increases as the coupling strength is increased. For $\lambda = 1$, we find that the HOMO-LUMO gap is about 1eV, a value typically observed for a long but finite polyene system, and which we will use for further calculations.

As a first step to understanding device response, we look at the equilib-

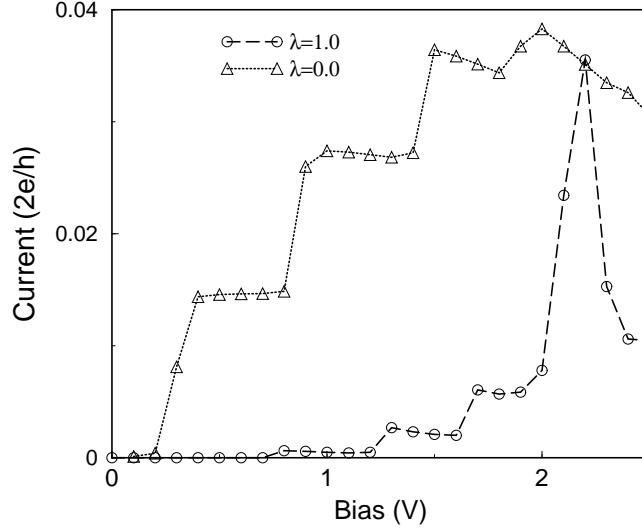


Figure 6: The current-voltage characteristics for a 20 sites molecular wire for the non-interacting case ($\lambda = 0$, triangles) and with electron-phonon coupling ($\lambda = 1$, circles).

rium transmission through the states around the Fermi energy(E_f). Quite interestingly, it shows that unlike in a pure non-interacting wire, the presence of electron-phonon coupling localizes the orbitals close to the Fermi energy, even in the absence of external bias. These are orbitals which are very important from transport point of view and we will show later, the consequences of such a localization. We next calculate the current-voltage (I-V) characteristics of the 20 sites molecular chain for $\lambda = 1$ as shown in Figure 6. As can be seen, the current increases by jumps for the noninteracting chain, and this staircase structure is quite well understood [30, 73]. However, with the inclusion of electron-phonon coupling, the I-V curve shows some remarkable features. Plateau structure is no more present at high bias and we find a sharply peaked NDR structure in the off-resonant condition. Interestingly, the magnitude of current at the critical bias is same with and without the

electron-phonon coupling.

To trace back the origin of this NDR behavior, we look at the variation of the low-energy levels (HOMO and LUMO) with bias, and find that in general the levels stabilize linearly with bias at small bias strength. But at the bias at which NDR is seen (critical bias), the HOMO and LUMO levels come very close up to a gap of $\sim 0.05\text{eV}$, after which they move farther apart. In the presence of strong electron-phonon coupling this accidental degeneracy between the levels induces mixing between the states that would be absent otherwise. Calculating other quantities such as the numerator of the Greens' function (which determines the nature of the plateau structure in the I-V) and the inverse participation ratio (IPR), we confirm that the NDR occurs when the system goes from one localized phase to another through a completely delocalized phase, at the critical bias, resulting in a sharp rise and fall in current.

We now explain this localization versus delocalization features of the levels as a function of bias with electron-phonon coupling. In the absence of electron-phonon coupling, all the bond lengths of the system are equal. The ground state wavefunction, corresponding to the HOMO level, consists of alternate symmetric and antisymmetric combinations of the atomic coefficients for the successive bonds across the chain. This corresponds to a particular parity configuration. However, since the molecular levels are placed in energy with alternate parity corresponding to the alternate energy levels, the LUMO will have exactly the opposite parity to the HOMO level [74]. The wavefunction for LUMO will then consist of opposite combinations of the atomic coefficients for the corresponding bonds. If the HOMO is written as

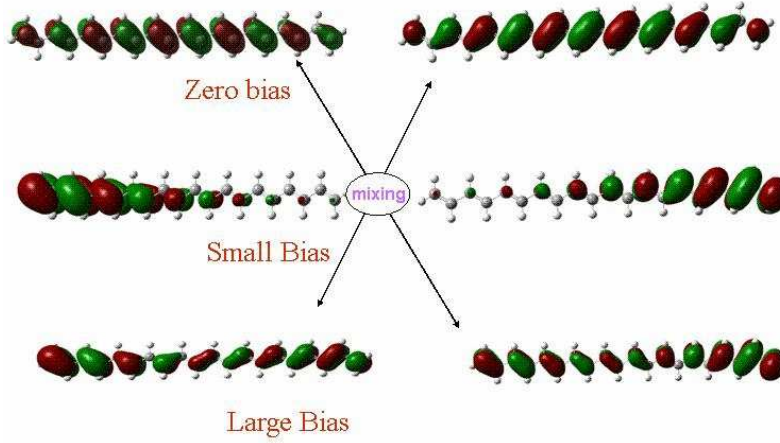


Figure 7: The HOMO (left) and LUMO (right) of the poly-acetylene chain of 20 atoms, in the presence of no, small and large electric field strengths.

$|++--++-->$, the LUMO then corresponds to $|+---++--++-->$, where the $+$ ($-$) corresponds to the sign of the atomic coefficients for the bond. However, as has been discussed, the system becomes dimerized with alternating long and short bonds once the electron-phonon coupling is introduced. The symmetric and antisymmetric combinations of the atomic coefficients in this case now correspond to the long and short bonds (or short and long bonds) respectively. In other words, if the HOMO is mapped to a lattice configuration with bond length variation as $= - = - = -$, the LUMO will then be $- = - = - =$. The large HOMO-LUMO gap at the zero bias condition is precisely the energy difference associated with the dimerized chain corresponding to these opposite symmetry combinations. This is also very clear from Figure 7, where we show the HOMO and LUMO orbitals for the inherently dimerized trans-polyacetylene system in the presence and absence of electric field. The system was optimized within the Gaussian 03 suite of programs, using the hybrid Becke 3 Lee-Yang-Parr (B3LYP) gradient corrected

exchange-correlation functional, at the 6-31G(d) basis set level. At zero bias, it is very evident that the HOMO is localized on the double bonds and the LUMO on the single bonds. As the bias is applied, the LUMO approaches the coefficient combinations corresponding to the HOMO and similarly the HOMO towards the LUMO, and at some critical bias, both of them have their energies corresponding to the lattice with equal bond lengths. Since for equal bond-lengths, the energy difference between these combinations is quite small, the HOMO and LUMO at the critical bias are almost degenerate. A glance at the orbitals in Figure 7, at small field, shows that the HOMO is getting localized in one half of the chain and the LUMO in the other half. At the critical bias, the quasi degeneracy of their energies, results in orbital mixing, leading to a complete delocalization over the entire chain. A complete confirmation of this is obtained from the I-V characteristics, where the current at the critical bias with electron-phonon coupling is exactly the same as that for the noninteracting system with equal bond-lengths (see Figure 6). With a further increase in field, it becomes very clear from Figure 7 that the HOMO orbitals are beginning to look like the LUMO and vice-versa, indicating that there is a change occurring from one insulating phase to the other, leading to the fall in current seen in the I-V characteristics.

We have also carried out self-consistent calculations combining the one-dimensional Poisson and Schrödinger equations, as described in the previous section. This is to explore the effect of the spatial electrostatic potential profile on the bond distortions and the transport across the chain. Since, in these calculations, the distortion pattern (δs) are self-consistently calculated at every bias, we find that, this even site half-filled system goes from one kind

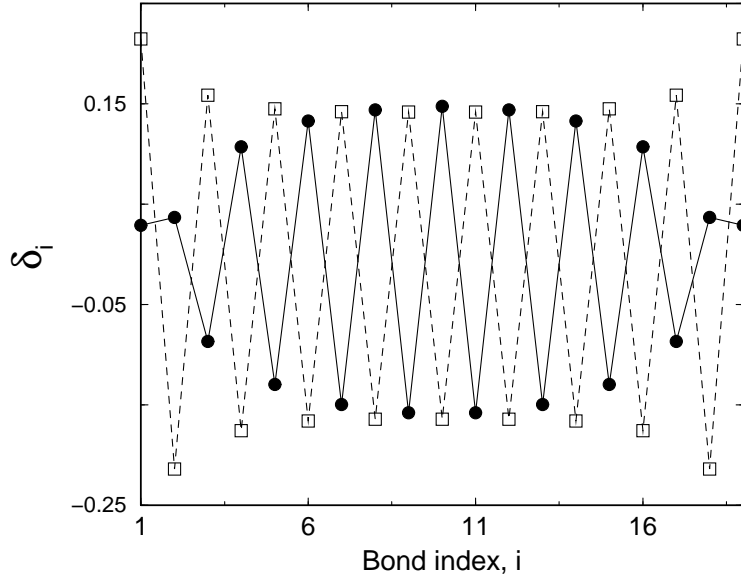


Figure 8: The bond-alternation parameter (δ_i) as a function of bond index, i , as obtained from the Poisson-Schrödinger self-consistent calculations for two values of the bias. Before NDR (bias=2.3V, squares) and after NDR (bias=2.4V, circles)[see Figure 6].

of dimerized phase to the other around this critical bias at which the energy levels show quasi-degenerate behavior. This is shown in Figure 8, where we have plotted distortion patterns at the bias values before and after the NDR peak in the I-V curve. Since the chain is an open system, the opposite dimerization pattern is evident only in the middle of the chain. At the critical bias, the nature of the potential profile also changes from RAMP, which is the profile we start with, to the tight binding potential profile (TBPF), which has large gradients towards the ends of the chains and zero gradient at the middle [37]. A similar mechanism for NDR was observed in an odd-sites system as well, where the notable point is that the ground state is a solitonic state. We find that the SOMO (singly occupied molecular orbital) also contributes to the mixing of energy levels at the critical bias, leading to NDR peaks [75].

To have a microscopic understanding of this NDR phenomenon, we also derive analytic expressions for the low-lying energies and wavefunctions, using time-independent perturbation theory, where the external bias acts as the perturbation. We consider two cases for our study - that of a uniform ($\delta t = 0$) chain and a partially dimerized chain, with the Hamiltonian, $H = -\sum_{i,\sigma}(t + (-1)^{i+1}\delta t)(a_{i,\sigma}^\dagger a_{i+1,\sigma} + hc)$, and derived expressions for the first and second order change in energies, caused by the presence of the field. The main point is that, in a dimer, the two sites contribute differently to the ground state of the partially dimerized chain, and thus gets intermixed by the external field creating a dipolar contribution that essentially allows the low-energy levels to approach each other. This leads to possibilities of NDR in the I-V characteristics of the dimerized chain as opposed to a uniform one. We refer the readers to Ref.[76] for more details of this study.

B. Role of donor-acceptor groups

Although our previous study throws some light on why NDR appears in conjugated systems, this subsection complements it by investigating the effect of the donor-acceptor groups in causing this. We find that not only NDR, but also the asymmetry that characterizes the I-V characteristics of these molecules, comes out naturally of our model [77]. And the simplicity of our parametrized model makes it very tractable and lends physical insight into the factors causing NDR.

Our model assumes that the part of the Tour molecule with the donor group (NH_2) has a negative on-site energy and that with the acceptor group (NO_2) has a positive on-site energy. The spatial variation of bias on the

structure, is considered (except in few cases considered later) to drop as a ramp function, varying linearly from one electrode to the other. With this potential, the energies for the dimer with Hamiltonian $H = \sum_{i=1,2} \epsilon_i (a_i^\dagger a_i) + \sum_i -t(a_i^\dagger a_{i+1} + hc)$, where ϵ_i is the on-site energy of site i and t is the hopping integral between the donor and acceptor, can be easily derived as:

$$E_{\pm} = \frac{\epsilon_1 + \epsilon_2 - V}{2} \mp \frac{\sqrt{9(\epsilon_1 - \epsilon_2)^2 + 36t^2 + V^2 + 6V(\epsilon_1 - \epsilon_2)}}{6}. \quad (8)$$

The coupling to the electrodes modifies the bare Greens function of the molecule, which can be written as

$$\begin{aligned} G_{12}(E, V) &= \frac{V - 3(\epsilon_2 - \epsilon_1) - \sqrt{(3(\epsilon_2 - \epsilon_1) - V)^2 + 36t^2}}{6t(E - E_1 + i\Sigma_L + i\Sigma_R)} \\ &+ \frac{V - 3(\epsilon_2 - \epsilon_1) + \sqrt{(3(\epsilon_2 - \epsilon_1) - V)^2 + 36t^2}}{6t(E - E_2 + i\Sigma_L + i\Sigma_R)} \end{aligned} \quad (9)$$

where Σ_L and Σ_R are the self-energies corresponding to the left and right electrodes. We calculate these quantities within the Newns-Anderson model, and subsequently current from the Landauer's formula.

At zero bias, as can be seen from Eqn.(8), with $V = 0$, presence of different on-site energies opens up a gap larger than that for a purely hopping model ($\epsilon_2 = \epsilon_1 = 0eV$) near the zero of energy indicating the preference of the electrons to stay at the atomic site with negative on-site energy. The equilibrium transmission is found to be large for purely hopping model since it corresponds to equal distribution of charges. With the inclusion of different on-site energies, the system becomes insulating due to charge transfer and

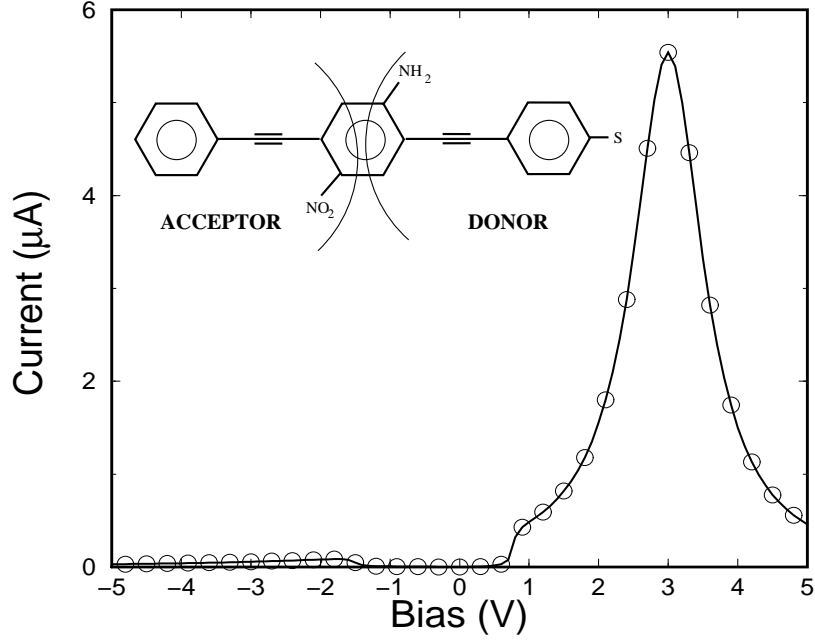


Figure 9: The current-voltage characteristics for the 2-site system for $\epsilon_2 = -\epsilon_1 = 0.5eV$ and $t = 0.1eV$. Inset is the Tour molecule.

the zero-bias transmission reduces due to this preferential charge localization,

Figure 9 shows the nature of the current-voltage characteristics with external bias. As can be seen, the current is negligible around the zero of energy and around a bias of $1V$, there is a small jump in the current. With increase in the forward bias, around a bias of $3V$, the current shows a sharp rise and fall, indicating strong Negative Differential Resistance (NDR). On the other hand, with increase in the reverse bias, the system continues to remain insulating with negligible current.

To understand the reasons for the NDR, we look at the variation of the energy levels (E_k) of the bare molecular dimer with bias (Figure 10(a)) and the numerator of the Greens function, $\langle 1|k\rangle\langle 2|k\rangle$ where $k = 1, 2$ are the eigenstates (Figure 10(b)), as a function of the external bias. With increase

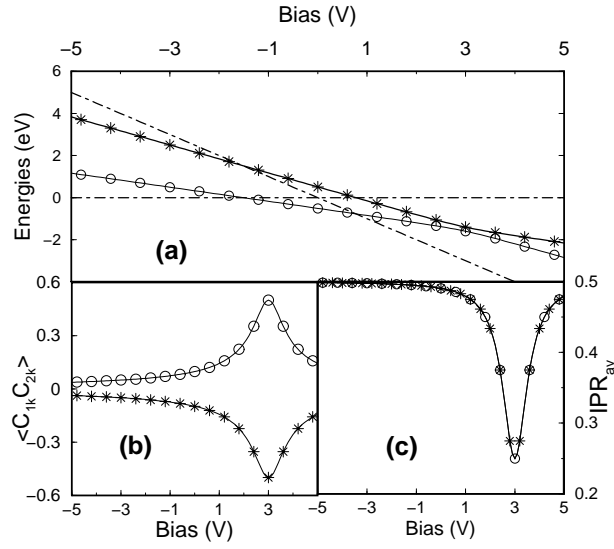


Figure 10: (a) The variation of the two levels (circles and stars) of the 2-site system with the applied bias, for $\epsilon_2 = -\epsilon_1 = 0.5eV, t = 0.1eV$. The dotted lines indicate the variation of the Fermi energies of the electrodes with bias. (b) The numerator of the Greens function matrix element for the corresponding energy levels shown in (a). 1 and 2 represent the site index and k specifies the corresponding level. (c) The IPR_{av} for the levels shown in (a).

in the forward bias, the energy levels come close to one another up to the critical bias V_c at which the NDR is seen, after which, they move farther away. In Figure 10(b), exactly around this V_c , the contribution to the dimer eigenstate coefficients from the sites increases quite sharply, indicating a more delocalized state. We also calculate the average inverse participation ratio (IPR_{av}) which defines the extent of localization for a given eigenstate, with energy E_k :

$$IPR_{av} = \frac{1}{D(E)} \frac{1}{N} \sum_k P_k^{-1} \delta(E - E_k) \quad (10)$$

where P_k^{-1} is the IPR, defined as $P_k^{-1} = \frac{1}{N} \sum_j |\psi(j, k)|^4$ where the j is the atomic site index and $D(E)$ is the density of states. Figure 10(c) shows a strong dip in the values of IPR_{av} around the critical bias confirming complete delocalization in the system, while at other values of the bias, IPR_{av} is much larger due to the localized nature of the eigenstates.

Since the model is exactly solvable, we quantify this critical bias V_c , by minimizing the gap between the energies with respect to the applied bias and obtain, $V_c = 3(\epsilon_2 - \epsilon_1)$, which is in accordance with our numerical data (for $\epsilon_1 = -0.5eV$ and $\epsilon_2 = 0.5eV$, we find $V_c \sim 3V$) [78]. [Using the values of the absolute electronegativities and hardness, the ionization potential difference between amino and nitro group is calculated to be of the order of 1.0 eV, same as what we considered for $\epsilon_2 - \epsilon_1$. Critical bias calculated from this, gives a reasonable comparison with experiments]. At this critical bias, the energies take the values $\mp t$, precisely the energies of the system with $\epsilon_1 = \epsilon_2 = 0$. However, with increase in the reverse bias, the energy levels start diverging away from their zero bias gap making the system more insulating, explaining

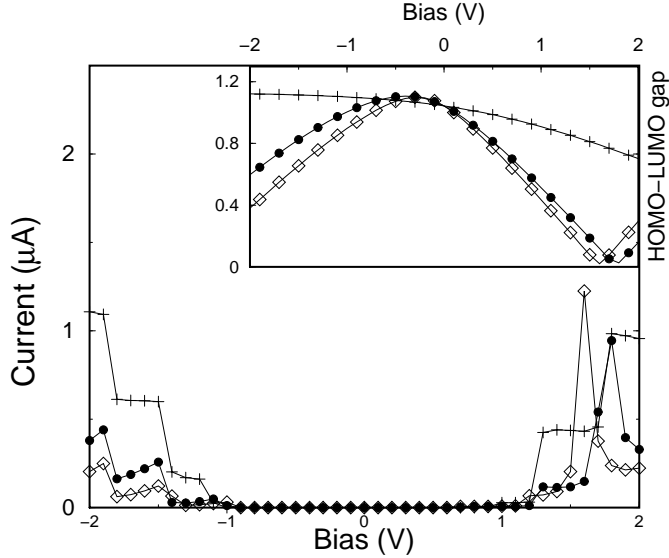


Figure 11: The I-V characteristics for the 20 site system with $\epsilon_2 = -\epsilon_1 = 0.5eV$ and $t = 1eV$ with ramp potential (diamonds), $l=2$ drop (plus), and $l=8$ drop (circles) close to the interface. The inset shows the variation of the HOMO-LUMO gap with bias for the three cases.

the small current that is observed in Figure 9 for negative bias.

We argue below physically what happens to the dimer in the presence of both the forward and reverse bias. Initially for small bias, as noted before, the system tends to accumulate its charge density at the site with lower on-site energy. Such a localization makes the system insulating. If this site is closer to the electrode with higher chemical potential, an increase in bias makes the charges tend to move towards the other site. When the bias equals the critical bias V_c , where the NDR is seen, the charge densities are equally distributed at both sites with no preference of one site over another, describing a situation where both the on-site energies are equal. Further increase of bias would localize the charges on the other site resembling an insulating dimer with its on-site energies interchanged, precisely the case as in the reverse bias situation.

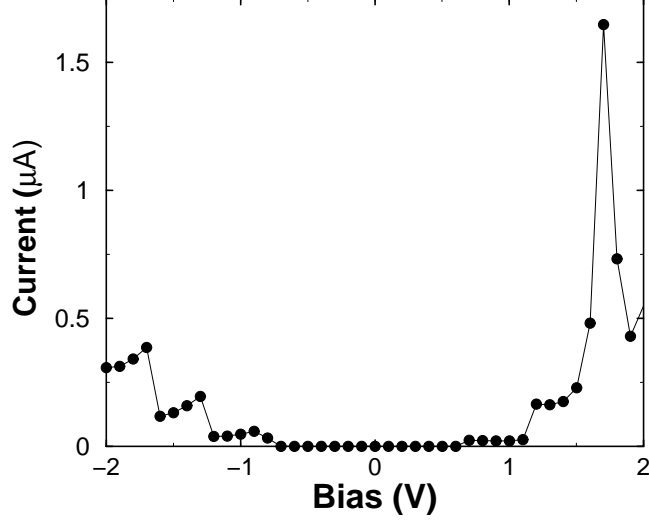


Figure 12: The I-V characteristics for the 20 site system with $t = 1eV$ and $\delta = 0.2eV$, where δ is the bond-alternation parameter. The system also has a donor and acceptor at symmetric sites 4, 17 with energies $\epsilon_4 = 0.5eV$ and $\epsilon_{17} = -0.5eV$.

Extending the dimer model to a N sites chain with alternating donor and acceptor sites, we can, from a perturbation view-point, derive an expression for the critical bias for NDR to be $V_c|_{t \rightarrow 0} = (\epsilon_2 - \epsilon_1)(N + 1)/(N - 1)$, with second order corrections due to the hopping term. Asymmetric I-V characteristics with NDR peaks appearing at different voltages in the forward and reverse bias directions is also a very notable point of this calculation. We have also considered different spatial variations of the bias, having larger gradients at the electrodes (as described in section II). As seen from Figure 11, we observe that, whenever there is a strong spatial dependence of the bias profile, the closing in of the HOMO and LUMO levels is more pronounced, and the NDR sharper. A profile with almost no spatial variation can even result in a no NDR situation.

In the long-chain limit, there is an implicit relation between variation in

on-site energies and the bond-length alternation (BLA). This is because in the $N \rightarrow \infty$ limit, the Fourier transformations of both the diagonal (on-site) and off diagonal (hopping) terms yield the same k (wavevector) components. The Tour molecules, as discussed before have both BLA (conjugation) together with donor and acceptor groups. We have already explained how BLA which dimerizes the system, gives rise to NDR. Interestingly, we find that acceptor ($+\epsilon$) and donor ($-\epsilon$) at some positions together with explicit dimerization also causes NDR and asymmetric I-V, as shown in Figure 12. Hence, we point out that, whether it is the explicit dimerization or two-sublattice structure, coupled with the voltage profile, it induces interchange of symmetry together with Landau quasi-degeneracy of the low-lying levels, leading to NDR.

IV Finite size correlated insulators

Having looked at the phenomenon of NDR in finite systems which are inherently insulating, either due to Peierls distortion or because of the presence of substituents, we naturally arrived at the question of whether such insulator-metal-insulator transitions would survive in systems which are insulating due to the presence of strong electron-electron interactions. Low-dimensional systems are almost always insulators, due to one or all of the reasons mentioned above and are commonly described by Peierls, Hubbard or related Hamiltonians [69, 79]. It is well-known that the ground state of a half-filled Hubbard system is a Mott insulator, and the effect of electric field on such a system has generated much interest in recent years due to the practical interest in tuning their dielectric and piezoelectric properties. In our work detailed below [80],

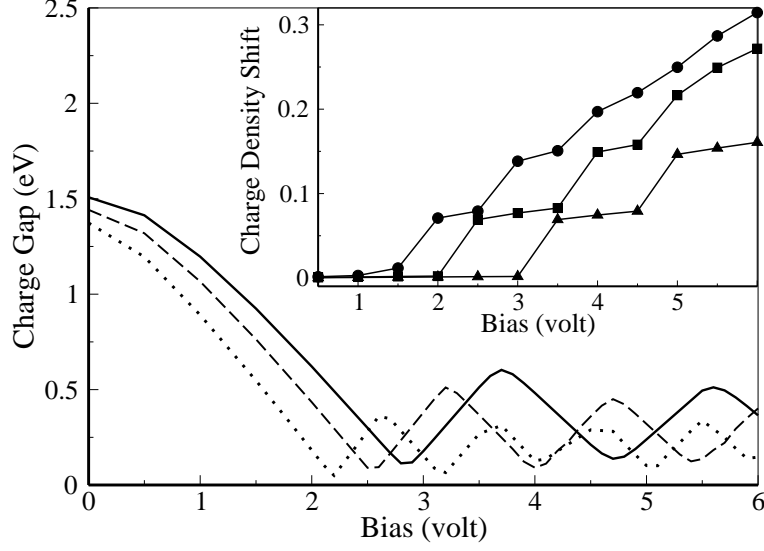


Figure 13: Charge gap vs bias for $N = 26$ (solid line), 30 (dashed line) and 40 (dotted line) for $U = 4$. Inset shows the average charge density shift per site as a function of bias for a system, $N = 30$ with $U = 3$ (circle), $U = 4$ (square) and $U = 5$ (triangle).

we investigate the effect of electric field on finite size correlated insulators, using the exact diagonalization method and obtain the ground and low-energy eigen states for various system sizes. We consider a one dimensional chain described by the Hubbard Hamiltonian,

$$H = \sum_i t(a_i^\dagger a_{i+1} + h.c) + U \sum_i n_{i\uparrow} n_{i\downarrow} \quad (11)$$

where t is the hopping term, U is the Hubbard term. We set $t = 1$ as the unit of energy. The external electric field (W) applied on the system, has the form of a ramp potential, adds an extra term $\sum_i W_i a_i^\dagger a_i$ to the above Hamiltonian. We perform calculation for various values of U and W .

The ground state of the Hamiltonian with nonzero U is a spin-density wave insulator with one electron at every site [81]. To understand the effect

of the external field on this system, the charge excitation gap defined as the difference between the energy required to add (μ_+) and remove (μ_-) electrons from the ground state [82], i.e, $\Delta_{charge} = \mu_+ - \mu_-$ is calculated. Here $\mu_+ = E(N+1) - E(N)$ and $\mu_- = E(N) - E(N-1)$. $E(N)$, $E(N+1)$ and $E(N-1)$ are the energies of the half-filled system and the systems with one extra and one less electron respectively. We plot in Figure 13 this charge gap as a function of bias for different system sizes, for some representative value of U . It can be clearly seen that the charge gap shows an oscillation with bias, going through a number of minima and maxima.

To understand the underlying reasons for this oscillation, we calculate the average charge density shift per site as a function of bias for various system sizes with several U values. In the inset of Figure 13, we present the charge density shift per site for the half-filled state of a finite chain with $N = 10$ for three representative values of U . At zero bias, the ground state charge density at every site of the system is the same and it continues to remain so up to the bias corresponding to the first minimum of the charge gap (Δ_{charge}). However, after that, it shows a large shift in the direction of bias, giving rise to charge inhomogeneities. The external bias tends to shift the charge densities towards one electrode with the nullification of U at the first Δ_{charge} minimum. However, beyond this, an increase in bias results in further hopping of charges leading to double occupancy of more sites, with electron repulsion overwhelming the kinetic stabilization, thereby increasing the energy gap. Further increase of bias nullifies this effective repulsion, resulting in the next charge gap minimum. Hence, such a variation in charge gap resulting in near-metallic (charge gap is not zero) behavior in various bias

regions is due to the interplay of the Hubbard repulsion, finite system size and the spatial gradient of the external bias. Interestingly, as can be seen from the figure, with increase in the size, the magnitude of bias corresponding to the first Δ_{charge} minimum reduces and the periodicity of occurrence of successive minima thereafter also narrows down. It is also evident from the inset that an increase in U requires a higher bias to shift the charge density, and thus the bias corresponding to the first Δ_{charge} minimum also increases.

For a simple understanding on the above breakdown phenomenon, we consider a 2 site Mott-insulator in presence of bias. With ramp potential, the first and the second site experiences the bias, $-\frac{W}{6}$ and $+\frac{W}{6}$ respectively. Out of 4^2 states, (a) the lowest energy of the one-electron states is $E_1 = -(\sqrt{(36t^2 + W^2)})/6$, while (b) for the 3 electron states it is, $E_3 = (6U - \sqrt{(36t^2 + W^2)})/6$. These bias dependent energies are stabilized with increase in bias, however, as expected, their energy difference is U for any W . The ground state of the half-filled system comprising of four basis states: (i) $|\uparrow\downarrow 0\rangle$, (ii) $|\uparrow\downarrow\rangle$, (iii) $|\downarrow\uparrow\rangle$ and (iv) $|0\uparrow\downarrow\rangle$. For $W = 0$, the ground state consists of singly occupied states (ii & iii), with second order (t^2/U) contribution from double occupancy site states (i & iv). However, as the bias increases, the state with double occupancy (state i) starts to contribute to the ground state energy (of the half-filled system), E_2 . It is because the external bias nullifies the Hubbard repulsion, leading to mixing of double and single occupancy states. This results in an increased hopping of electrons and hence a closing of the repulsion induced charge gap at W_c . Beyond W_c , the state with double occupancy (state i) starts gaining prominence and the energy E_2 stabilizes with bias. This results in an increasing value of μ_+ and

a decreasing value of μ_- and hence a rise in the charge gap leading to an insulating state again. Although in this simple 2-site model, the states with one-electron never faces the effect of U , it could, however, capture the essence of the insulator-near metal transition, albeit qualitatively.

These insulator-near metal-insulator transitions strongly indicate that the current through these systems would show a number of NDR peaks[83].

V NDR in double quantum dots in the coulomb blockade regime

In this section, we focus on the NDR phenomenon that has recently been observed in double quantum dots in the low temperature, weak molecule-electrode coupling limit, also known as the coulomb blockade regime [84]. Theoretical studies of NDR in this regime have also started gaining a lot of prominence in recent times [85, 86, 87]. Mean field descriptions are known to usually fail here, as electron charging energies are very high as compared to the broadenings due to the electrode coupling [88, 89]. Also, since these methods, combined with standard non-equilibrium Greens function (NEGF) treatment of transport are perturbative in the interaction parameter, they cannot capture the transitions between the spectrum of neutral and excited states, which can lead to a variety of interesting features in the I-V characteristics. The formalism that has now come to be used widely to capture molecular transport in the coulomb blockade regime is the master or rate equation method [90, 91]. Here, we use this formalism to study a system consisting of a donor and acceptor in the coulomb blockade regime. Tak-

ing cue from our mean-field transport studies on such systems which showed NDR behavior, as discussed before [77], here we explore the role of strong correlations in determining their transport in the single electron charging regime [92]. The rate equation formalism describes transport through a correlated system with many-body eigenstates. The presence of coulomb interactions results in occupation probabilities of each many body state that cannot be factorized as the product of the occupation probabilities of each single electron level. Hence, in this case, the full rate-equation problem, where the occupation probability of each many-body state is treated as an independent variable is solved, neglecting off-diagonal coherences. In this method, the transition rate $\Sigma_{s' \rightarrow s}$ from the many-body state s' to s , involving transitions between states differing by one electron, is calculated up to linear order in Γ (which is the bare electron tunneling rate between the system and the electrode), using Fermi's golden rule (from second-order perturbation theory) as [90, 91],

$$\begin{aligned}\Sigma_{s' \rightarrow s}^{L+} &= \Gamma f_L(E_s - E'_s) \sum_{\sigma} | \langle s | C_{1\sigma}^{\dagger} | s' \rangle |^2 \\ \Sigma_{s' \rightarrow s}^{R+} &= \Gamma f_R(E_s - E'_s) \sum_{\sigma} | \langle s | C_{N\sigma}^{\dagger} | s' \rangle |^2\end{aligned}\tag{12}$$

with a corresponding equation for $\Sigma_{s \rightarrow s'}^{L-}$ and $\Sigma_{s \rightarrow s'}^{R-}$ obtained by replacing $f_{L,R}(E_s - E'_s)$ by $(1 - f_{L,R}(E_s - E'_s))$. Here, $+/-$ correspond to the creation/annihilation of an electron inside the molecule due to electron movement from/to left (L) or right (R) electrode. We have also assumed that the creation and annihilation happen only at the terminal sites. The total

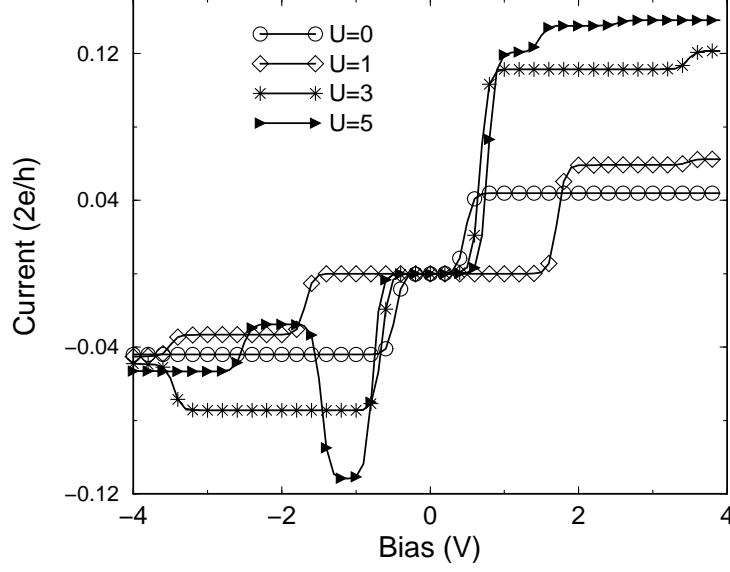


Figure 14: The I-V characteristics of the 2 site donor-acceptor system obtained using the rate equation approach, for various values of the Hubbard parameter U . Here, $\epsilon_1 = -\epsilon_2 = 2.0\text{eV}$, $t = 1.0\text{eV}$.

transition rate is then obtained as, $\Sigma_{s \rightarrow s'} = \Sigma_{s \rightarrow s'}^{L+} + \Sigma_{s \rightarrow s'}^{R+} + \Sigma_{s \rightarrow s'}^{L-} + \Sigma_{s \rightarrow s'}^{R-}$. The non-equilibrium probability P_s of occurrence of each many-body state s , is obtained by solving the set of independent rate equations defined by $\dot{P}_s = \sum_{s'} \Sigma_{s' \rightarrow s} P_{s'} - \Sigma_{s \rightarrow s'} P_s$ through the stationarity condition $\dot{P}_s = 0$ at steady state. This results in a homogeneous set of equations of the size of the Fock space. Taking advantage of the normalization condition $\sum_s P_s = 1$, we obtain linear equations, which can be solved using well-known linear algebraic methods. The steady state probabilities are then used to obtain the terminal current as ($\alpha = L/R$ electrode),

$$I_\alpha = \frac{e}{\hbar} \sum_{s,s'} \Sigma_{s' \rightarrow s}^{\alpha+} P_{s'} - \Sigma_{s \rightarrow s'}^{\alpha-} P_s \quad (13)$$

There have been previous theoretical studies on donor-acceptor double

dot systems where strong rectification has been observed [93], and others which showed NDR with variation in the molecule-electrode coupling [87, 94] or due to a detuning of the molecular levels [94]. Another recent study has attempted to establish conditions obeyed by the parameters involved, to observe a collapse in the current [95]. However, in our study, we find that some subtle changes in the parameters do result in NDR peaks in regimes where the conditions may not be followed strictly. Our Hamiltonian for the two site system is written as,

$$H = \sum_{i=1}^2 \epsilon_i (a_i^\dagger a_i) + \sum_{\sigma} -t (a_{1\sigma}^\dagger a_{2\sigma} + hc) + U \sum_{i=1}^2 n_{i\uparrow} n_{i\downarrow}$$

where t is the hopping strength between the donor and acceptor, $\epsilon_{1,2}$ are the on-site energies and U is the Hubbard interaction between electrons at the same site. For obtaining current, for every value of U , the Fermi energy (E_F) is chosen as the gate bias value which ensures that the two electron state is the ground state. The Fermi energy is also placed in such a way that we observe transitions from the ground state to the state with one less electron. Results however, would look similar for transitions to the state with one more electron.

In Figure 14, we plot the current-voltage characteristics of the system, for various values of the Hubbard parameter. As can be seen clearly, low values of U result in step-like features in the I-V, due to transitions from the 2 electron ($2e^-$) singlet ground state to the 1 electron ($1e^-$) doublet states and then to the state with no electron. Interestingly, with increase in U , a rise and fall in current (a NDR feature) is observed for negative values of bias.

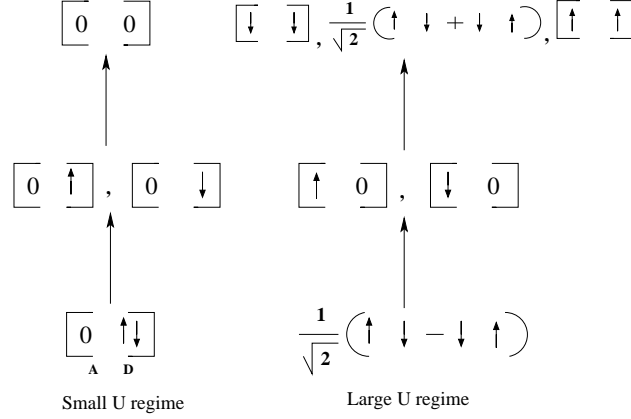


Figure 15: A schematic describing the transitions between the states of the donor-acceptor system, in the small and large U regimes.

An analysis of the probabilities shows that this happens when the second jump in the system occurs from the $1e^-$ doublet to a higher excitation of the $2e^-$ state, namely the triplet states, instead of to the state with no electron. This is because, when U is small, the ground state gives higher preference to the state with $2e^-$ of opposite spins at the site with lower on-site energy. This allows annihilation of an electron by the electrode followed by one more annihilation leading to a transition from the $2e^-$ singlet to the $1e^-$ doublet to the state with 0 electron. When U increases, however, the ground state gives more weightage to the state with $1e^-$ at the donor and one at the acceptor (see Figure 15). This allows for one annihilation from the ground state to the $1e^-$ doublet state, followed by a creation from the same electrode to the $2e^-$ triplet state, which has the same energy as the 0 electron state. Since the current at any electrode is calculated at steady state as the difference between the outgoing and incoming current (see Eqn.13), this transition results in a reduction in current leading to the negative differential resistance peak (also known as spin-blockade).

The I-V is asymmetric because of the inherent asymmetry in the system comprising of a donor and an acceptor. This becomes very apparent for larger U values for which NDR appears only at one polarity of the applied bias. This is because, the transition from $1e^-$ doublet to the $2e^-$ triplet through a creation at the acceptor is less feasible than at the donor.

VI Conclusions

In conclusion, we have attempted to present the effects of electric field on molecular systems between macroscopic electrodes, to gain an understanding of some of the factors that determine how the I-V characteristics of a nanoscale system would look. As a first step, we have elaborated the importance of the potential profile i.e the way the external applied field would fall across the molecule, and how the presence of electron correlations in the molecule can drastically change its shape, thereby changing the device response along-with it. Furthermore, highlighting the negative differential resistance (NDR) phenomena in molecules that has captivated the attention of researchers due to its immediate application in switching devices, we have shown that the presence of a two sublattice structure, caused either by a lattice distortion or substituents with a large dipolar strength, can result in NDR, when the external field has a strong spatial dependence. We find that the ratio t (hopping integral) : $\epsilon_2 - \epsilon_1$ (measure of the dipolar character), is very crucial in determining the nature of the I-V characteristics. Three features, namely (1) the critical bias (2) the sharpness of the NDR peak and (3) the extent of asymmetry in the I-V curves are sensitive to this ratio. Al-

though a common thread between all the known factors governing NDR is yet to be understood, we think that our reasoning even encompasses other existing explanations such as bias driven conformational changes, reduction of the acceptor to donor, as well as the bias driven changes in electrode-molecule coupling, all of which would equivalently result in a change in the electronic structure caused by the external bias. Our study also highlights the importance of a strong spatial dependence of the potential profile to obtain a sharp NDR peak. A natural question of whether such an NDR will survive when the system is insulating due to presence of electron-electron interactions in them, led us to study correlated insulators in the presence of field, where too we have shown that insulator-near metal-insulator transitions can be brought about by the spatially varying external bias, thus opening up possibilities for switching in these systems. Additionally, we have elucidated how a variation of these interaction strengths in double quantum dots can result in device responses varying from normal coulomb blockade to NDR.

It is mandatory to say at this point that most of our studies have assumed tunneling as the mechanism of transport and calculations have been performed in the coherent transport regime. However, the field itself is rich in studies on incoherent as well as activated transport characteristics. Experimental observation of phase loss in DNA junctions [96] and theoretical studies based on the Buttiker probe [97] or generalized master equations [67] are just some of the efforts in this direction, and a proper understanding of decoherence in condensed phase transport is still a challenge [98]. Electron-electron interactions, which in molecular transport are the source of Coulomb blockade phenomena, have been explored in some of the later

parts of this review, however, there have been many observations of both the Coulomb blockade and the Kondo effect in molecular junctions, and very often they are accompanied by vibrational features as well, which make transport phenomena more interesting with advanced technological applications [99]. Theoretical approaches based on the equation of motion method [100] or Fock space formalism [101] have also begun to appear to gain understanding of this regime. Although, we have discussed mainly about one of the technologically useful non-linear phenomena, namely, Negative differential resistance, other phenomena such as multistability and hysteresis, which arise out of structural changes in a molecule during transport together with inelastic processes due to interactions at different energy and length scales in organic, inorganic or hybrid systems still remain the subjects of active current research [102, 103, 104, 105].

VII Acknowledgements

SD acknowledges the CSIR for the research fellowship and SKP acknowledges the research support from DST and CSIR, Govt. of India.

References

- [1] Moore, G. *Electronics* **1965**, 38, 114-117.
- [2] Ghosh, A. W.; Damle, P. S.; Datta, S.; Nitzan, A. *MRS Bulletin* **June 2004**, 391-395.
- [3] Heath, J. R.; Ratner, M. A. *Physics Today* **May 2003**, 43-49.

- [4] Dutta, A.; Pati, S. K. *Chem. Soc. Rev.* **2006**, *35*, 1305.
- [5] Carroll, R. L.; Gorman, C. B. *Angew. Chem. Int. Ed.* **2002**, *41*, 4378.
- [6] Aviram, A.; Ratner, M. A. *Chem. Phys. Lett.* **1974**, *29*, 277.
- [7] Metzger, R. M.; Chen, B.; Höpfner, U.; M. V. Lakshmikantham, D. V.; Kawai, T.; Wu, X. L.; Tachibana, H.; Hughes, T. V.; Sakurai, H.; Baldwin, J. W.; Hosch, C.; Cava, M. P.; Brehmer, L.; Ashwell, G. J. *J. Am. Chem. Soc.* **1997**, .
- [8] Reed, M. A.; Zhou, C.; Muller, C. J.; Burgin, T. P.; Tour, J. M. *Science* **1997**, *278*, 252.
- [9] Reichert, J.; Ochs, R.; Beckman, D.; Weber, H. B.; Mayor, M.; Löhneysen, H. *Phys. Rev. Lett.* **2002**, *88*, 176804.
- [10] Kushmerick, J. G.; Holt, D. B.; Yang, J. C.; Naciri, J.; Moore, M. H.; Shashidar, R. *Phys. Rev. Lett.* **2002**, *89*, 086802.
- [11] Blum, A. S.; Kushmerick, J. G.; Long, D. P.; Patterson, C. H.; Yang, J. C.; Henderson, J. C.; Yao, Y.; Tour, J. M.; Shashidar, R.; Ratna, B. R. *Nat. Mater.* **2005**, *4*, 167.
- [12] Cai, L.; Cabassi, M. A.; Yoon, H.; Cabarcos, O. M.; McGuinness, C. L.; Flatt, A. K.; Allara, D. L.; Tour, J. M.; Mayer, T. S. *Nano Lett.* **2005**, *5*, 2365.
- [13] Chen, F.; He, J.; Nuckolls, C.; Roberts, T.; Klare, J. E.; Lindsay, S. *Nano Lett.* **2005**, *5*, 503.

- [14] Gust, D.; Moore, T. A.; Moore, A. L. *Chem. Commun.* **2006**, 11, 1169.
- [15] Xu, B.; Xiao, X.; Yang, X.; Zang, L.; Tao, N. *J. Am. Chem. Soc.* **2005**, 127, 2386.
- [16] Yoneya, N.; Watanabe, E.; Tsukagoshi, K.; Aoyagi, Y. *Appl. Phys. Lett.* **2001**, 79, 1465.
- [17] Bockrath, M.; Cobden, D. H.; McEuen, P. L.; Chopra, N. G.; Zettl, A.; Thess, A.; Smalley, R. E. *Science* **1997**, 275, 1922.
- [18] Nygard, J.; Cobden, D. H.; Lindelof, P. E. *Nature* **2000**, 408, 342.
- [19] Babic, B.; Kontos, T.; Schnenberger, C. *Phys. Rev. B* **2004**, 70, 235419.
- [20] Tans, S. J.; Verschueren, A. R. M.; Dekker, C. *Nature* **1998**, 393, 49.
- [21] Braun, E.; Eichen, Y.; Sivan, U.; Ben-Yoseph, G. *Nature* **1998**, 391, 775.
- [22] Fink, H. W.; Schonenberger, C. *Nature* **1999**, 398, 407.
- [23] Porath, D.; Bezryadin, A.; de Vries, S.; Dekker, C. *Nature* **2000**, 403, 635.
- [24] Storm, A. J.; van Noort, S.; de Vries, S.; Dekker, C. *Appl. Phys. Lett.* **2001**, 79, 3881.
- [25] Kasumov, A. Y.; Kociak, M.; Gueron, B.; Reulet, B.; Volkov, V. T.; D. V. Klinov, H. B. *Science* **2001**, 291, 280.

- [26] Maruccio, G.; Biasco, A.; Visconti, P.; Bramanti, A.; Pompa, P. P.; Calabi, F.; Cingolani, R.; Rinaldi, R.; Corni, S.; Felice, R. D.; Molinari, E.; Verbeet, M. P.; Canters, G. W. *Adv. Mater.* **2005**, *17*, 816.
- [27] Tao, N. *Journal of Chemical Education* **2005**, *82*, 720.
- [28] Datta, S. *Electronic Transport in Mesoscopic Systems*; Cambridge University Press: Cambridge, UK, 1995.
- [29] Landauer, R. *IBM J. Res. Dev.* **1957**, *1*, 223.
- [30] Zahid, F.; Paulsson, M.; Datta, S. *Advanced Semiconductors and Organic Nano-Techniques*; H. Morkoc, Academic Press: NewYork, 2003.
- [31] Mujica, V.; Kemp, M.; Ratner, M. A. *J. Chem. Phys.* **1994**, *101*, 6849.
- [32] Brandbyge, M.; Taylor, J.; Stokbro, K.; Mozos, J. L.; Ordejon, P. *Phys. Rev. B* **2002**, *65*, 165401.
- [33] Calzolari, A.; Marzari, N.; Souza, I.; Nardelli, M. B. *Phys. Rev. B* **2004**, *69*, 035108.
- [34] Taylor, J.; Guo, H.; Wang, J. *Phys. Rev. B* **2001**, *63*, 245407.
- [35] Palacios, J. J.; Perez-Jimenez, A. J.; Louis, E.; SanFabian, E. *Phys. Rev. B* **2002**, *66*, 035322.
- [36] Datta, S.; Tian, W.; Hong, S.; Reifenberger, R.; Henderson, J. I.; Kubiak, C. P. *Phys. Rev. Lett* **1997**, *79*, 2530.

- [37] Mujica, V.; Roitberg, A. E.; Ratner, M. A. *J. Chem. Phys.* **2000**, *112*, 6834.
- [38] Lakshmi, S.; Pati, S. K. *Proc. of the Indian Acad. of Sci. (Chem. Sci.)* **2003**, *115*, 533.
- [39] Pati, S. K. *J. Chem. Phys.* **2003**, *118*, 6529.
- [40] Fradkin, E. *Field Theories of Condensed Matter Systems (Advanced Books Classics S.)*; Westview Press, 1998.
- [41] Chen, J.; Reed, M. A.; Rawlett, A. M.; Tour, J. M. *Science* **1999**, *286*, 1550.
- [42] Chen, J.; Wang, W.; Reed, M. A.; Rawlett, A. M.; Price, D. W.; Tour, J. M. *Appl. Phys. Lett.* **2000**, *77*, 1224.
- [43] Reed, M. A.; Chen, J.; Rawlett, A. M.; Price, D. W.; Tour, J. M. *Appl. Phys. Lett.* **2001**, *78*, 3735.
- [44] Xiao, X.; Nagahara, L. A.; Rawlett, A. W.; Tao, N. *J. Am. Chem. Soc.* **2005**, *127*, 9235.
- [45] He, J.; Lindsay, S. M. *J. Am. Chem. Soc.* **2005**, *127*, 11932.
- [46] Zhang, C.; Du, M.-H.; Cheng, H.-P.; Zhang, X.-G.; Roitberg, A. E.; Krause, J. L. *Phys. Rev. Lett.* **2004**, *92*, 158301.
- [47] He, J.; Lindsay, S. M. <http://arxiv.org/abs/0708.1041> **2007**.
- [48] Li, Y. F.; Hatakeyama, R.; Kaneko, T.; Kato, T.; Okada, T. *Appl. Phys. Lett.* **2007**, *90*, 073106.

- [49] Kiehl, R. A.; Le, J. D.; Candra, P.; Hoye, R. C.; Hoye, T. R. *Appl. Phys. Lett.* **2006**, 88, 172102.
- [50] Guisinger, N. P.; Greene, M. E.; Basu, R.; Baluch, A. S.; Hersam, M. C. *Nano Lett.* **2004**, 4, 55.
- [51] Larade, B.; Taylor, J.; Mehrez, H.; Guo, H. *Phys. Rev. B.* **2001**, 64, 075420.
- [52] Seminario, J. M.; Araujo, R. A.; Yan, L. *J. Phys. Chem. B* **2004**, 108, 6915.
- [53] Dalglish, H.; Kirczenow, G. *Nano Lett.* **2006**, 6, 1274.
- [54] Liu, R.; Ke, S.-H.; Baranger, H. U.; Yang, W. *J. Am. Chem. Soc.* **2006**, 128, 6274.
- [55] Seminario, J. M.; Zacarias, A. G.; Tour, J. M. *J. Am. Chem. Soc.* **2000**, 122, 3015.
- [56] Seminario, J. M.; Zacarias, A. G.; Derosa, P. A. *J. Chem. Phys.* **2002**, 116, 1671.
- [57] Han, J. E.; Crespi, V. H. *Appl. Phys. Lett.* **2001**, 79, 2829.
- [58] Xiao, X.; Nagahara, L. A.; Rawlett, A. M.; Tao, N. *J. Mater. Chem.* **2005**, 127, 9235.
- [59] Taylor, J.; Brandbyge, M.; Strokbø, K. *Phys. Rev. B* **2003**, 68, 121101.

- [60] Karzazi, Y.; Cornil, J.; Bredas, J. L. *J. Am. Chem. Soc.* **2001**, *123*, 10076.
- [61] Cornil, J.; Karzazi, Y.; Bredas, J. L. *J. Am. Chem. Soc.* **2002**, *124*, 3516.
- [62] Pati, R.; Karna, S. P. *Phys. Rev. B* **2004**, *69*, 155419.
- [63] Shi, X.; Zheng, X.; Dai, Z.; Wang, Y.; Zeng, Z. *J. Phys. Chem. B.* **2005**, *109*, 3334.
- [64] Peierls, R. E. *Quantum Theory of Solids*; Oxford University Press: Oxford, England, 1956.
- [65] Ness, H.; Fisher, A. J. *Phys. Rev. Lett.* **1999**, *83*, 452; *Proc. Natl. Acad. Sci. USA* **2005**, *102*, 8826.
- [66] Montgomery, M. J.; Todorov, T. N. *J. Phys.: Condens. Matter* **2003**, *15*, 8781.
- [67] Segal, D.; Nitzan, A. *Chem Phys.* **2001**, *268*, 315; Petrov, E. G.; Zelinskyy, Y. R.; May, V. *J. Phys. Chem. B.* **2002**, *106*, 3092.
- [68] Lakshmi, S.; Pati, S. K. *J. Chem. Phys.* **2004**, *121*, 11998.
- [69] Su, W. P.; Schreiffer, J. R.; Heeger, A. J. *Phys. Rev. Lett.* **1979**, *42*, 171.
- [70] Su, W. P.; Schreiffer, J. R.; Heeger, A. J. *Phys. Rev. B* **1980**, *22*, 2099.
- [71] Newns, D. M. *Phys. Rev.* **1969**, *178*, 1123.

- [72] Anderson, P. W. *Phys. Rev.* **1961**, *124*, 41.
- [73] Mujica, V.; Kemp, M.; Ratner, M. A. *J. Chem. Phys.* **1996**, *104*, 7296.
- [74] Keiss, H. G. *Conjugated Conducting Polymers*; Springer-Verlag: Berlin, 1992.
- [75] Lakshmi, S.; Pati, S. K. *Pramana - Journal of Physics* **2005**, *65*, 593.
- [76] Sengupta, S.; Lakshmi, S.; Pati, S. K. *J. Phys.: Condens. Matter* **2006**, *18*, 9189.
- [77] Lakshmi, S.; Pati, S. K. *Phys. Rev. B.* **2005**, *72*, 193410.
- [78] Pearson, R. G. *Inorg. Chem.* **1988**, *27*, 734.
- [79] Gutzwiller, M. C. *Phys. Rev. Lett.* **1963**, *10*, 159.
- [80] Dutta, S.; Lakshmi, S.; Pati, S. K. *J. Phys.: Condens. Matter* **2007**, *19*, 322201.
- [81] Campbell, D. K.; Baeriswyl, D.; Majumdar, S. *Conjugated Conducting Polymers*; Springer-Verlag: New York, 1992.
- [82] Lieb, E.; Wu, F. *Phys. Rev. Lett.* **1968**, *20*, 1445.
- [83] Bandyopadhyay, A.; Acharya, S. *Proc. Nat. Acad. Sci.* **2008**, *105*, 3668.
- [84] Ono, K.; Austing, D. G.; Tokura, Y.; Tarucha, S. *Science* **2002**, *297*, 1313.

- [85] Hettler, M. H.; Wenzel, W.; Wegewijs, M. R.; Schoeller, H. *Phys. Rev. Lett.* **2003**, *90*, 076805.
- [86] Nguyen, V. H.; Nguyen, V. L.; Dollfus, P. *Appl. Phys. Lett.* **2005**, *87*, 123107.
- [87] Thielmann, A.; Hettler, M. H.; König, J.; Schön, G. *Phys. Rev. B.* **2005**, *71*, 045341.
- [88] Datta, S. *Nanotechnology* **2004**, *15*, S433.
- [89] Muralidharan, B.; Ghosh, A. W.; Datta, S. *Phys. Rev. B* **2006**, *73*, 155410.
- [90] Hettler, M. H.; Schoeller, H.; Wenzel, W. *Europhys. Lett.* **2002**, *57*, 571.
- [91] Beenakker, C. W. J. *Phys. Rev. B* **1991**, *44*, 1646.
- [92] Lakshmi, S.; Pati, S. K. *submitted* .
- [93] Song, B.; Ryndyk, D. A.; Cuniberti, G. *Phys. Rev. B.* **2007**, *76*, 045408.
- [94] Aghassi, J.; Thielmann, A.; Hettler, M. H.; Schön, G. *Phys. Rev. B.* **2006**, *73*, 195323.
- [95] Muralidharan, B.; Datta, S. *Phys. Rev. B.* **2007**, *76*, 035432.
- [96] Xu, B.; Zhang, P.; Li, X.; Tao, N. *Nano Lett.* **2004**, *4*, 1105.
- [97] Datta, S. *J. Phys.: Condens. Matter.* **1990**, *2*, 8023; Neofotistos, G.; Lake, R.; Datta, S. *Phys. Rev. B.* **1991**, *43*, 2442;

- [98] Galperin, M.; Ratner, M. A.; Nitzan, A. *J. Phys.: Condens Matter* **2007**, *19*, 103201.
- [99] Yu, L. H.; Natelson, D. *Nano Lett.* **2004**, *4*, 79; Park, J.; Pasupathy, A. N.; Goldsmith, J. I.; Chang, C.; Yaish, Y.; Petta, J. R.; Rinkoski, M.; Sethna, J. P.; Abruna, H. D.; McEuen, P. L.; Ralph, D. C. *Nature* **2002**, *417*, 722.
- [100] Krawiec, M.; Wysokinski, K. I. *Phys. Rev. B.* **2002**, *66*, 165408.
- [101] Muralidharan, B.; Ghosh, A. W.; Pati, S. K.; Datta, S. *IEEE Transac. on Nanotech.* **2007**, *6*, 536.
- [102] Keane, Z. K.; Ciszek, J. W.; Tour, J. M.; Natelson, D. *Nano Lett.* **2006**, *6*, 1518.
- [103] Mohanta, K.; Batabyal, S. K. Pal, A. J. *Adv. Func. Matter.* **2008**, *18*, 687.
- [104] Kiehl, R. A.; Le, J. D.; Candra, P.; Hoye, R. C.; Hoye, T. R. *Appl. Phys. Lett.* **2006**, *88*, 172102.
- [105] Galperin, M.; Ratner, M. A.; Nitzan, A. *Nano Lett.* **2004**, *5*, 125.